Nicotinamide riboside modulates the reactive species interactome, bioenergetic status and proteomic landscape in a brain-region-specific manner

Alejandro Marmolejo-Garza, Laurent Chatre, Deborah L Croteau, Alejandro Herron-Bedoya, Minh Danh Anh Luu, Benoit Bernay, Julien Pontin, Vilhelm A Bohr, Erik Boddeke, Amalia M Dolga

Neurobiology of Disease 200 (2024) 106645

Contents lists available at ScienceDirect

Neurobiology of Disease

journal homepage: www.elsevier.com/locate/ynbdi

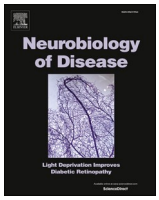

Nicotinamide riboside modulates the reactive species interactome, bioenergetic status and proteomic landscape in a brain-region-specific manner

Alejandro Marmolejo-Garza [a,b], Laurent Chatre [c], Deborah L. Croteau [d,e], Alejandro Herron-Bedoya [a], Minh Danh Anh Luu [a], Benoit Bernay [f], Julien Pontin [f], Vilhelm A. Bohr [d,g,h], Erik Boddeke [b,h], Amalia M. Dolga [a,*]

[a] Faculty of Science and Engineering, Department of Molecular Pharmacology, Groningen Research Institute of Pharmacy (GRIP), University of Groningen, 9713, AV, Groningen, the Netherlands
[b] Department of Biomedical Sciences of Cells & Systems, section Molecular Neurobiology, Faculty of Medical Sciences, University of Groningen, University Medical Center Groningen, Groningen, the Netherlands
[c] Université de Caen Normandie, CNRS, Normandie Université, ISTCT, UMR6030, GIP CYCERON, F-14000 Caen, France
[d] Section on DNA repair, National Institute on Aging, 251 Bayview Blvd, Baltimore, MD, USA
[e] Laboratory of Genetics and Genomics, Computational Biology and Genomics Core, National Institute on Aging, 251 Bayview Blvd, Baltimore, USA
[f] Université de Caen Normandie, US EMerode, Plateform Proteogen, F-14000 Caen, France
[g] Center for Healthy Aging, Department of Cellular and Molecular Medicine, SUND, University of Copenhagen, 2200, Copenhagen N, Denmark
[h] Department of Cellular and Molecular Medicine, Center for Healthy Aging, University of Copenhagen, Copenhagen, Denmark

ARTICLE INFO

Keywords:
Nicotinamide riboside
Reactive species Interactome
Alzheimer's disease
Mitochondria
Metabolism
Neurodegeneration
Aging
Bioenergetics

SUMMARY

Nicotinamide riboside (NR), a precursor of nicotinamide adenine dinucleotide (NAD+), has robust cognitive benefits and alleviates neuroinflammation in Alzheimer's Disease (AD) mouse models without decreasing beta-amyloid plaque pathology. Such effects may be mediated by the reactive species interactome (RSI), at the metabolome level. In this study, we employed *in vitro* and *in vivo* models of oxidative stress, aging and AD to profile the effects of NR on neuronal survival, RSI, and the whole proteome characterization of cortex and hippocampus. RSI analysis yielded a complex modulation upon NR treatment. We constructed protein co-expression networks and correlated them to NR treatment and all measured reactive species. We observed brain-area specific effects of NR on co-expressed protein modules of oxidative phosphorylation, fatty acid oxidation, and neurotransmitter regulation pathways, which correlated with RSI components. The current study contributes to the understanding of modulation of the metabolome, specifically after NR treatment in AD and how it may play disease-modifying roles.

1. Introduction

Recent studies have highlighted the intricate interplay between proteostasis, mitochondrial dysfunction, and the dysregulation of reactive species in the pathogenesis of neurodegenerative diseases (Pinho et al., 2020; Fourcade et al., 2015; Joy et al., 2021; Molenaars et al., 2020; Korovila et al., 2017; Huang et al., 2020), including Alzheimer's Disease (AD) (Molenaars et al., 2020; Beck et al., 2016). In addition to amyloid-beta and tau pathology, dysfunctions in mitochondrial bioenergetics and redox homeostasis have emerged as critical contributors to neurodegeneration (Swerdlow et al., 2014; Swerdlow and Khan, 2004; Swerdlow et al., 2010; Wilkins and Swerdlow, 2016). In AD, mitochondria are not only the primary source of cellular energy production, but also key regulators of redox signaling and oxidative stress (Misrani et al., 2021). Mitochondrial impairments, including defects in oxidative phosphorylation, electron transport chain, and impaired mitochondrial dynamics, have been observed in both familial and sporadic forms of AD. These mitochondrial abnormalities can lead to the generation of reactive oxygen species (ROS), reactive nitrogen species (RNS), reactive sulfur species (RSS), and reactive carbonyl species (RCS)

* Corresponding author at: Faculty of Science and Engineering, Groningen Research Institute of Pharmacy, Department of Molecular Pharmacology, University of Groningen, Antonius Deusinglaan 1, Groningen, the Netherlands.
E-mail address: a.m.dolga@rug.nl (A.M. Dolga).

https://doi.org/10.1016/j.nbd.2024.106645
Received 1 July 2024; Received in revised form 17 August 2024; Accepted 19 August 2024
Available online 22 August 2024

(Malard et al., 2021), which, in turn, contribute to neuronal damage and degeneration. This oxidation-reduction system which consists of ROS, RNS, RSS and RCS is defined as the reactive species interactome (RSI).

Unbiased approaches to profile the proteomic disturbances in the AD brain have detected protein network modules such as MAPK signaling, metabolism, and matrisome which are not observed in transcriptomic screens (Johnson et al., 2022). Earlier studies have detected protein modules that are specific to microglia and astrocyte activation (Johnson et al., 2020). In the brain, proteostatic disturbances may be linked to dysregulation of reactive species as they form a vicious loop where one could potentiate the effects of the other (Korovila et al., 2017; Malard et al., 2021). Today, there are no therapeutic approaches to target the recently described protein modules in AD. However, a plethora of efforts aim to target reactive species within neurodegenerative diseases (Chen et al., 2023; Marmolejo-Garza et al., 2023; Marmolejo-Garza et al., 2022; Richter et al., 2015; Honrath et al., 2017; Dolga et al., 2013). All in all, targeting the reactive species may be a promising disease-modifying therapeutic strategy.

DNA damage and impaired DNA repair mechanisms have been implicated in the pathogenesis of AD (Lin et al., 2020; Weissman et al., 2007) leading to genomic instability and neuronal death. Deficiencies in base excision repair (BER) DNA repair enzymes, such as polymerase β (Polβ) proteins have been reported in AD brains. Among the BER mechanisms, Polβ is the rate-limiting for repair in AD brains (Weissman et al., 2007). The accumulation of DNA damage can further exacerbate mitochondrial dysfunction and oxidative stress, creating another vicious cycle of cellular damage and neurodegeneration. 3xTg AD mice express mutated amyloid precursor protein (APP), presenilin-1 and Tau, and develop age-dependent extracellular Aβ plaques, contain intracellular Tau accumulation, have increased oxidative stress and cognitive deficit, while there is no neuronal degeneration. In 2015, we generated the 3xTg mice heterozygous for Polβ (3xPB) and reported that these mice exhibit neuronal death, and the RNAseq data showed more transcriptomic similarities with human AD patients than 3xTg AD mice or mice heterozygous for polymerase Polβ (HT).

Based on all aforementioned findings, targeting mitochondrial bioenergetics, redox homeostasis, and DNA repair pathways has emerged as a promising therapeutic strategy for AD (Trombetta-Lima et al., 2021) and other neurodegenerative diseases (Bhatti et al., 2022). Nicotinamide riboside (NR), a precursor of nicotinamide adenine dinucleotide (NAD+), is being utilized for its neuroprotective effect (Yujun et al., 2018; Vreones et al., 2023). NR supplementation has been shown to enhance mitochondrial function, increase ATP production, and alleviate oxidative damage in preclinical models of neurodegeneration (Fang et al., 2016). Furthermore, NR has been reported to activate sirtuins (Curry et al., 2023), a family of NAD + -dependent deacetylases involved in regulating cellular metabolism, stress response, and longevity. NAD+ supplementation has been shown to reduce neuroinflammation and cell senescence, as well as to improve the cognitive phenotype in the 3xPB and other transgenic models of AD (Liu et al., 2013; Yujun et al., 2018; Gong et al., 2013). Interestingly, NR treatment does not affect Aβ production or formation *in vivo* and *in vitro (*Yujun et al., 2018*)* suggesting that its protective effects are mainly mediated by decreased neuroinflammation and oxidative stress. Oxidative stress has been shown to decrease in human AD fibroblasts upon NR treatment (Yujun et al., 2018). Moreover, oxytosis/ferroptosis pathways converge at mitochondria, with increased reactive species formation, and recent findings suggest that these pathways contribute to the pathology of AD (Marmolejo-Garza et al., 2022; Trombetta-Lima et al., 2021; Maher et al., 2018; Majerníková et al., 2021). We and others have demonstrated that ferroptosis induction occurs in aging and in AD patients and models (Chen et al., 2023; Marmolejo-Garza et al., 2023; Majerníková et al., 2021) and it can be prevented *in vitro (*Marmolejo-Garza et al., *2023)*. One example of this approach is the targeting of the mitochondrial calcium uniporter complex. Detailed characterization of the reactive species interactome, including oxygen, nitrogen, sulfur and carbonyl for these AD models as well as their modulation upon NR treatment has not been performed.

In this study, we investigated the effects of NR on oxytosis/ferroptosis-induced cell death *in vitro* and followed up with *in vivo* experiments with NR supplementation on brain-region-specific bioenergetics and redox disturbances in the 3xPB mice (mouse model of AD with DNA repair deficiency). We employed a combination of biochemical assays, mass spectrometry-based proteomic analysis, and weighted correlation network analysis (WGCNA) to characterize the molecular changes associated with NR treatment in the cortex and hippocampus of 3xTgAD/HT PolB mice (3xPB). Our findings provide insight into the mechanisms underlying the therapeutic potential of NR in mitigating mitochondrial dysfunction, redox state modulation, and proteostasis in AD pathology. By integrating these findings, we sought to contribute to the development of targeted therapeutic interventions aimed at preserving mitochondrial function, redox homeostasis, and proteostasis in neurodegenerative diseases.

2. Results

2.1. NR supplementation prevents oxidative distress-related cell death ferroptosis in primary cortical neurons

To investigate the protective potential of NR in oxidative distress-driven cell death such as ferroptosis, we treated primary cortical neurons (PCNs) with the GPX4 inhibitor, RAS-selective lethal 3 (RSL3). GPX4 is the glutathione peroxidase 4 which protects the cells against hydrogen peroxide and lipid peroxidation. We first investigated whether RSL3 can induce degeneration and fragmentation of the neuronal network. We observed a decrease in the calcein-positive neuronal network area when PCNs were treated with RSL3. Treatment of PCN with NR (20 μM) mediated a prevention of such deficit when the PCNs were cotreated with RSL3 (Fig. 1A). The decrease and degeneration of the neuronal network elicited by RSL3 treatment and the effect of the NR co-treatment were statistically significant (Fig. 1B,C). Together, these data demonstrate the potential of NR against strong oxidative distress *in vitro* in cortical neurons.

2.2. 3xPB mice exhibit increased ATP abundance in cortex and hippocampi upon NR supplementation

To assess the effect of NR replenishment on bioenergetics *in vivo,* we treated 16–18-mo-old 3xTgAD/Polβ$^{+/-}$ (3xPB) mice with 12 mM NR for 8 weeks. Polβ$^{+/-}$ (HT), and WT were included as controls. Behavioral analyses of 3xPB mice revealed severe deficits in memory, learning, and cell death compared to their corresponding control mice (Yujun et al., 2018; Sykora et al., 2015), while NR treatment was able to prevent such changes (Hou et al., 2021). We have included the HT (mice heterozygous for Polβ) as a control on the same Polβ deficiency background as the 3xPB mice. We then performed an array of biochemical assays to profile bioenergetics and the RSI in the cortex and hippocampi of these animals, as it was suggested previously that NR could mediate suppressive effects on inflammation in both hippocampi and cortex (Yujun et al., 2018). Firstly, the total ATP abundance was not affected by the Polβ$^{+/-}$ depletion when compared to the WT controls in both cortex and hippocampus. We observed no difference in the abundance of ATP in the 3xPB mice when compared to WT or HT mice in both brain areas. However, the cortex and the hippocampus of NR-treated mice had significantly increased total ATP levels compared to their untreated controls (Fig. 2A & 2B). These data demonstrated that NR treatment is able to increase the ATP content in the cortex and hippocampi of 3xPB mice.

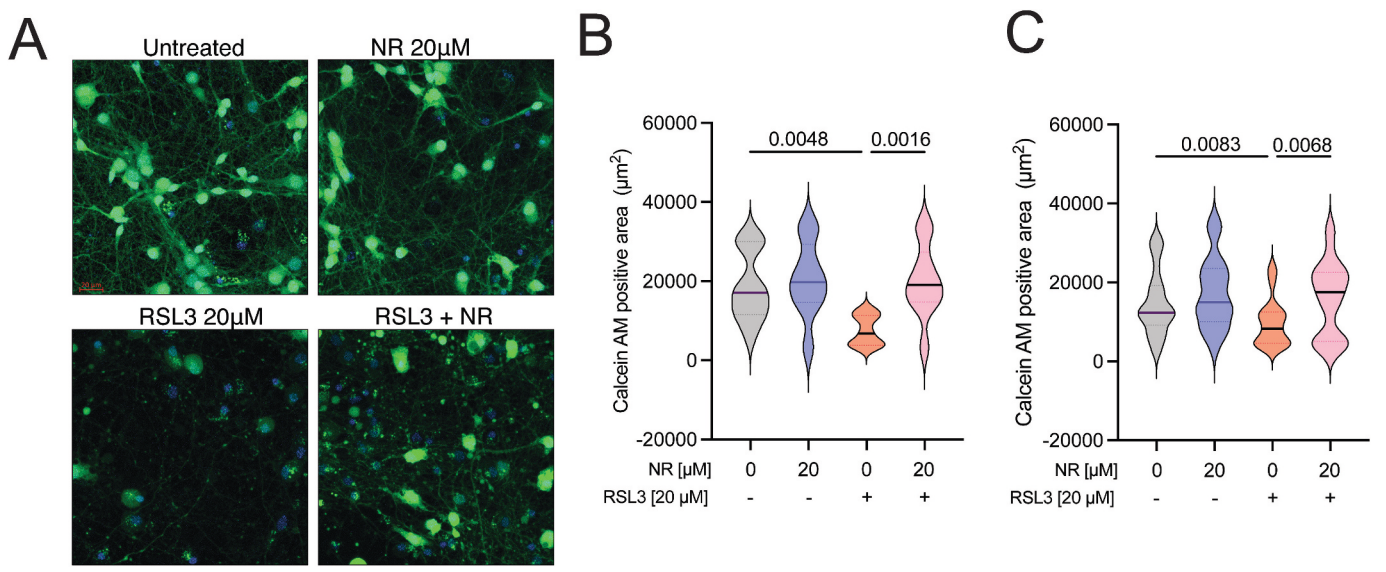

Fig. 1. Effect of NR on RSL3-induced PCN cell death.
A. Representative micrographs of Calcein-stained primary cortical neurons. Scale bar equals 20 μm.
B. Quantification of Calcein-AM area of a representative experiment. Untreated ($N = 10$), RSL3 (N = 10), NR ($N = 9$), RSL3 + NR (N = 10). C. Quantification of Calcein-AM areas of three independent experiments. Untreated ($N = 25$), RSL3 ($N = 30$), NR ($N = 24$), RSL3 + NR (N = 30). Data are presented as violin plots depicting data distributions, median and quartiles. Statistical significance was calculated by two-way Analysis of Variance (ANOVA) with a Dunnett's multiple comparisons test.

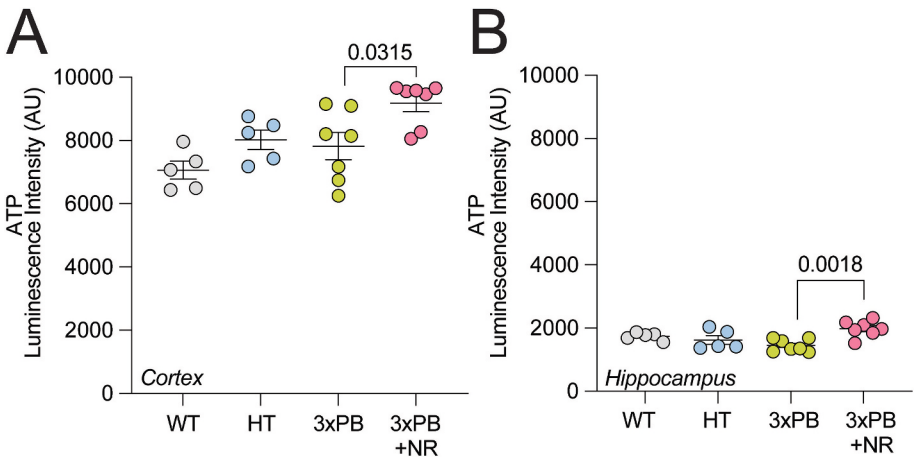

Fig. 2. ATP measurements in NR-treated 3xPB mice.
A. ATP measurements of cortex lysates of AD mice. $N = 5$–7 animals per group.
B. ATP measurements of hippocampus and cortex of AD mice. N = 5–7 animals per group. Data are presented as individual animal's data as scatter dotplots with mean ± SEM. All p values were calculated by One-way ANOVA with Tukey's multiple comparisons test.

2.3. 3xPB mice exhibit decreased ROS in the cortex upon NR supplementation

To assess the reactive species interactome, we first profiled the abundance of ROS, namely the superoxide anion (O_2^-), and hydrogen peroxide (H_2O_2) in the cortex and hippocampus of all treated and untreated mice. ROS are generated by using the precursors O_2 to form O_2^-, later H_2O_2 and other derivative species (Malard et al., 2021). The main enzyme that catalyzes the reduction of O_2^- to H_2O_2 is superoxide dismutase (SOD). We observed a robust increase of O_2^- in the Polβ$^{+/-}$ mice compared to the WT controls in both brain areas (Fig. 3A). The same effect of the Polβ$^{+/-}$ mutation on O_2^- was also observed in the hippocampus (Fig. 3B), and these findings are highlighting the contribution of the HT polb mutation to oxidative distress. The treatment with NR significantly decreased O_2^- in cortex but not in the hippocampus. (H_2O_2 was increased in the HT background compared to controls in both brain areas (Fig. 3C & 3D). The 3xPB animals had significantly lower H_2O_2 than their heterozygous controls in cortex but not in the hippocampus. NR treatment significantly decreased H_2O_2 in the cortex (Fig. 3C) but increased it in the hippocampus (Fig. 3D). All in all, the aging phenotype of HT mice recapitulates the increase in ROS in both brain areas, cortex and hippocampus, while the changes in ROS abundance following NR treatment were found to be brain-region specific.

2.4. 3xTG/PB mice do not exhibit dysregulated RNS in cortex and hippocampus and upon NR supplementation NO is upregulated in the hippocampus

RNS metabolism derives from L-arginine and NO synthase (NOS). NO

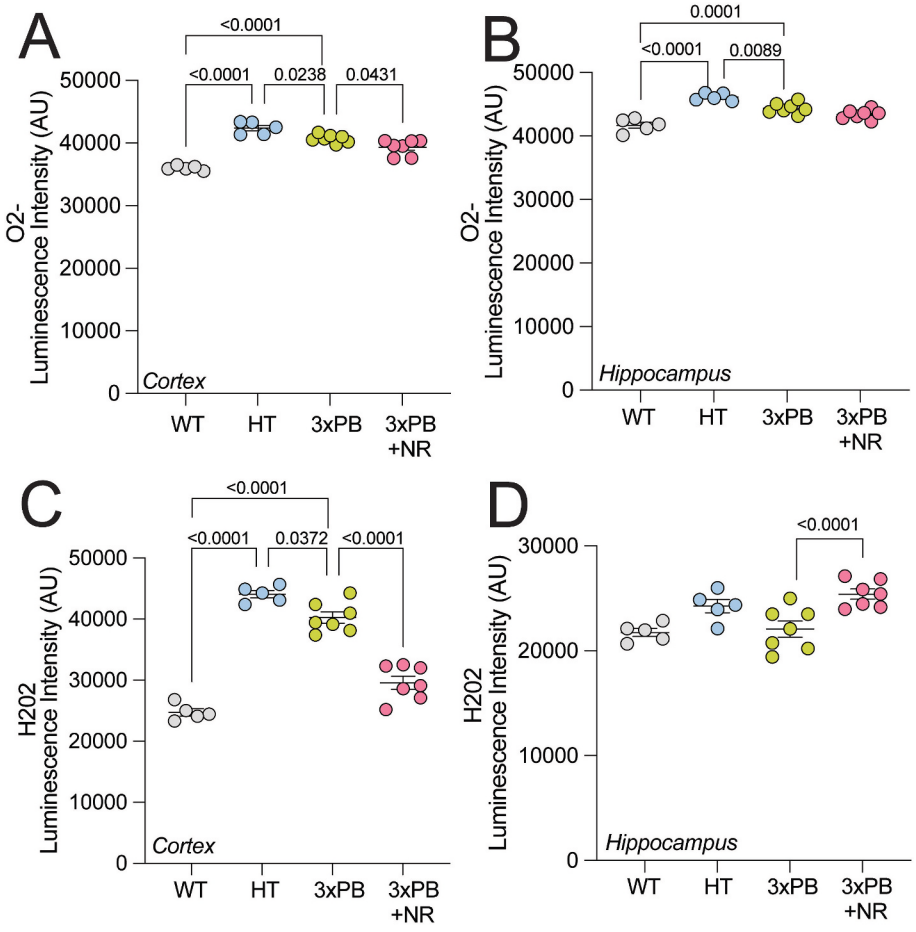

Fig. 3. Measurement of Reactive Oxygen Species $O2^{-}$ and H_2O_2.
A. O_2^- abundance in cortex of NR treated 3xPB mice.
B. O_2^- abundance in hippocampus of NR treated 3xPB mice.
C. H_2O_2 abundance in cortex of NR treated 3xPB mice.
D. H_2O_2 abundance in hippocampus of NR treated 3xPB mice.
For all plots, $N = 5–7$ animals. *P* values were calculated by one-way ANOVA with Tukey's multiple comparisons test. Data are presented as individual animal's data as scatter dotplots with mean ± SEM.

is generated by three isoforms of NOS: neuronal, inducible, and endothelial NOS. NO reacts with O_2^- to form $ONOO^-$, linking ROS and RNS metabolism. We report here that the HT background does not elicit significant changes in NO in cortex and hippocampus (Fig. 4A & 4B). Similarly, the 3xPB animals did not exhibit significant changes in NO compared to the HT group. Interestingly, the NR treatment increased the abundance of NO in hippocampus, but not cortex in the 3xTG/PB mice (Fig. 4A & 4B). When we measured $ONOO^-$, we observed no significant difference across all experimental groups (Fig. 4C & 4D). Together, these data point out that NR treatment has a brain-region-specific effect on NO in 3xTG/PB mice hippocampi and no effect on $ONOO^-$.

2.5. 3xPB mice exhibit increased RSS in cortex, which is recovered in a brain-area-dependent manner upon NR treatment

RSS comprises derivatives of hydrogen sulfide (H_2S), which is generated by thioredoxin (TRX). Once produced, H_2S regulates many pathways including the redox system, the glutathione system and mitochondrial bioenergetic with both beneficial and deleterious effects. Metabolism of H_2S into polysulfides (H_2S_n) is a major RSS event impacting many pathways. In the cortex, we observed an important increase of H_2S in the 3xPB animals compared to their HT controls (Fig. 4E). This increase was abolished with the NR treatment (Fig. 4E). For hippocampi, we only observed an increase in H_2S in the HT background when compared to their WT littermates (Fig. 4F). We also measured H_2S_n and observed a significant increase upon NR treatment in hippocampus only (Fig. 4H) and not in cortex (Fig. 4G). These results suggest that NR treatment targets the RSS metabolism, *via* H_2S in cortex and through H_2S_n in hippocampi.

2.6. 3xPB mice exhibit decreased reactive carbonyl species (RCS) in cortex and increased RCS in hippocampus upon NR treatment

Many carbonyl species from lipid peroxidation or glycoxidation are reactive and have the potential of disrupting function of other proteins and enzymes. These RCS include malondialdehydes (MDA), methylglyoxal (MGO), and 4-hydroxy-trans-2nonenal (4-HNE). We employed a fluorescence assay that employs NBD-H to form highly fluorescent derivatives to quantify RCS abundance in brains regions of our mouse cohort. We observed no changes upon NR treatment in the cortex (Fig. 4I) and an increase in hippocampus (Fig. 4J). These data suggest that NR treatment elicits brain-region-specific effects on RCS.

2.7. Effects of Polβ$^{+/-}$ on the proteome of the cortex and hippocampi

Given that we identified important differences in the reactive species interactome when comparing wild-type and heterozygous Polb mutant mice, we decided to profile their proteomic landscape before

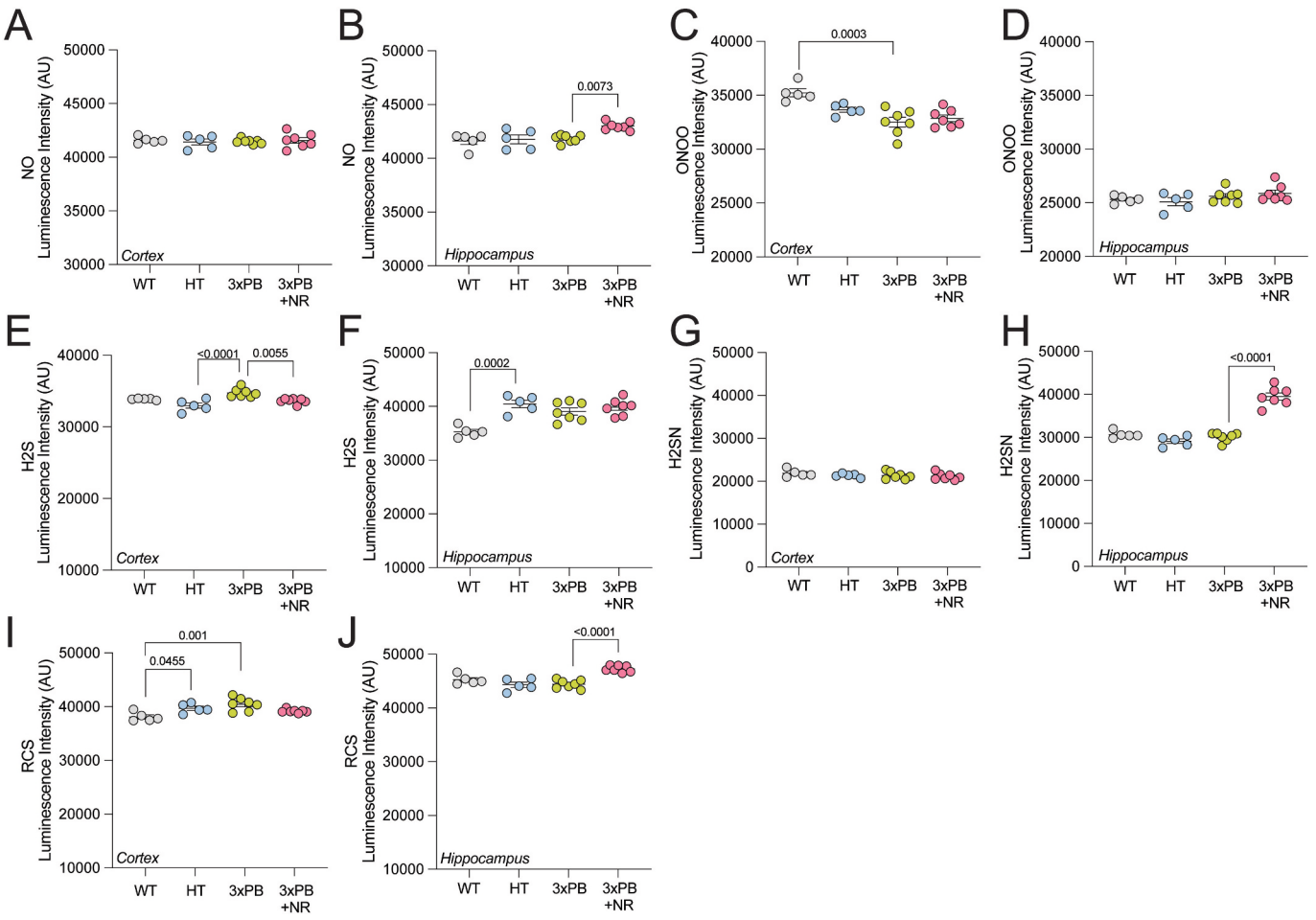

Fig. 4. Measurement of Reactive Nitrogen, Sulfur, and Carbonyl Species.
A. NO^- abundance in cortex of NR treated 3xPB mice.
B. NO^- abundance in hippocampus of NR treated 3xPB mice.
C. $ONOO^-$ abundance in cortex of NR treated 3xPB mice.
D. $ONOO^-$ abundance in hippocampus of NR treated 3xPB mice.
E. H_2S abundance in cortex of NR treated 3xPB mice.
F. H_2S abundance in hippocampus of NR treated 3xPB mice.
G. H_2S_n abundance in cortex of NR treated 3xPB mice.
H. H_2S_n abundance in hippocampus of NR treated 3xPB mice.
I. RCS abundance in cortex of NR treated 3xPB mice.
J. RCS abundance in hippocampus of NR treated 3xPB mice. For all plots, $N = 5–7$ animals, P values were calculated by one-way ANOVA. Data are presented as individual animals as scatter dotplots with mean ± SEM.

investigating the effects of NR supplementation. For cortex and hippocampi areas, we performed label-free quantitation mass spectrometry proteomics. We performed downstream differential expression analysis for both brain areas of HT and WT mice. In the cortex, TXNDC17, GPM6B, and SPRN were detected as statistically-significant upregulated proteins (Fig. 5A & 5B). TXNDC17 is the Thioredoxin Domain Containing 17. Thioredoxins play cytoprotective roles against various oxidative stress conditions as they have radical-scavenging activity (Bjørklund et al., 2022). GPM6B is the neuronal tetraspan glycoprotein M6B which belongs to the proteolipid protein (PLP) expressed by astrocytes, oligodendrocytes and neurons. SPRN is the shadow of prion protein, a prion-like protein that has neuroprotective activity (Daude et al., 2015). The proteome analysis revealed that UBAI3, PPP1CC, and SLC25A31 were downregulated in the HT mice (Fig. 5A & 5B, Table S1). TUBAL3 is the tubulin alpha like 3, a major component of microtubules which has been associated with AD (Zhang et al., 2018). PP1CC is the protein phosphatase 1 catalytic subunit gamma, a ubiquitous serine/threonine phosphatase that regulates cell division. SLC25A31 is solute carrier family 25 member 31, an ADP:ATP antiporter that mediates import of ADP into the mitochondrial matrix for ATP synthesis, and export of ATP to fuel the cell (Clémençon et al., 2013). In our study in the hippocampi, only GPT2 was upregulated, while RPL14 was the only downregulated protein (Fig. 5C & 5D, Table S4). GPT2 is the glutamic—pyruvic transaminase 2, which catalyzes the reversible transamination between alanine and 2-oxoglutarate to form pyruvate and glutamate. RPL14 is the Ribosomal protein L14, a component of the large ribosomal subunit. Although the proteomic changes of the brain areas of the HT mice are discreet, the proteins that remained statistically significant reflect processes such as upregulation of radical-scavenging and decreased neuronal density.

2.8. The cortex proteome of 3xPB mice is dysregulated when compared to their littermate controls and NR supplementation does not elicit robust proteomic changes

The proteomic landscape upon AD hallmarks has been reported to be

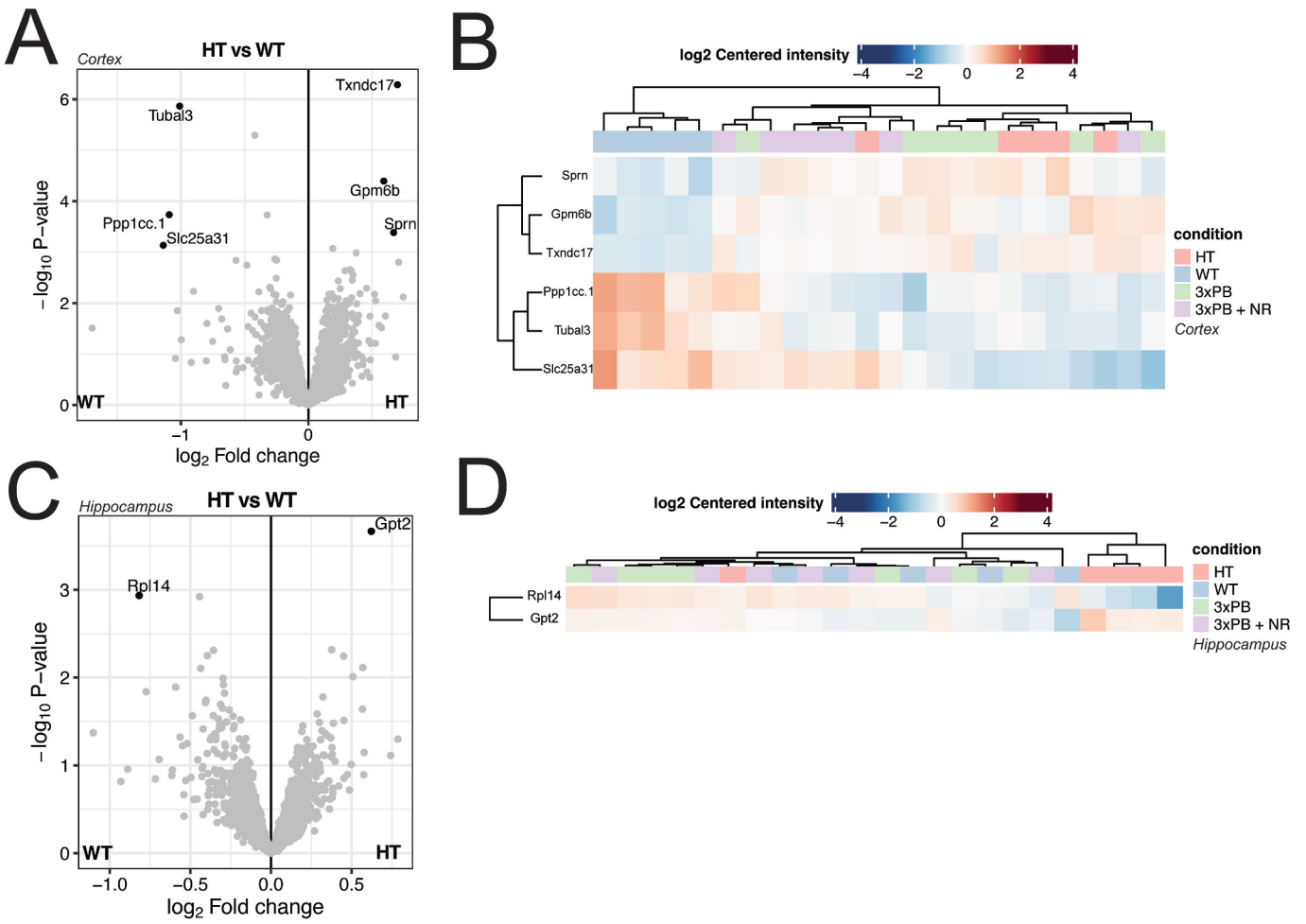

Fig. 5. Proteomic comparison between HT and WT brain areas.
A. Volcano plot depicting differentially expressed proteins in the cortex of HT and WT mice.
B. Heatmap depicting the proteomic abundances of SPRN, GPM6B, TXNDC17, PPP1CC, TUBAL3, SLC25A31.
C. Volcano plot depicting differentially expressed proteins in the hippocampi of polb HT and WT mice.
D. Heatmap depicting the proteomic abundances of RPL14, GPT2.

dysregulated in patient cohorts and animal models (Johnson et al., 2022; Johnson et al., 2020; Xiong et al., 2019; Kühl et al., 2017). We aimed to investigate the proteomic landscape of the AD model 3xPB and compare with their littermate controls which were only harboring the Polβ$^{+/-}$ background. These mice exhibit upregulation of GABRA2, PZP, ADI1, MPST, GLO1, NME3, ITIH4, HDH5, and C3 among others. GABRA2 is an alpha subunit of GABA-1 receptors. PZP is the pregnancy zone protein, which has stabilizing properties on misfolded proteins including amyloid β peptide (Cater et al., 2019; Nijholt et al., 2015). ADI1 is the Acireductone Dioxygenase 1 which belongs to the family of metal-binding enzymes involved in methionine salvage. MPST is the mercaptopyruvate sulfurtransferase, which transfers sulfur ions to cyanide or to other thiol compounds acting as an antioxidant. GLO1 is the glyoxalase 1, which forms S-lactoyl-glutathione from methylglyoxal condensation and reduced glutathione. NME is the nucleoside diphosphate kinase 3 which is involved in the synthesis of nucleoside triphosphates. ITIH4 is the inter-Alpha-Trypsin Inhibitor Heavy Chain 4, an acute-phase protein involved in inflammation. HDH5 is the Haloacid dehalogenase like hydrolase domain containing 5, which is predicted to be involved in glycerophospholipid biosynthetic process. C3 is the complement component 3, a protein that is required for the activation of the complement system. TTC38 was downregulated in 3xPB mice (Fig. 6A & Fig. 6B, Table S2). TTC38 is the Tetratricopeptide Repeat Domain 38, a protein that is located in exosomes. Differential expression analysis between the cortex of NR-treated and untreated 3xPB mice yielded no statistically-significant dysregulated proteins after multiple-testing correction (Fig. 6C, Table S3). Nevertheless, we filtered for the top 100 proteins with the smallest raw *p*-values (these proteins have the most significantly-different distributions across this comparison) and observed enrichment of processes related to metabolism of lipids and synthesis of palmitic acid among others (Fig. 6D). These data demonstrate that the 3xPB proteomic landscape recapitulates some classically AD-associated changes and that treatment with NR, although it does not modify the proteome robustly, may contribute to metabolic changes related to lipid processing.

2.9. The hippocampi proteome of 3xPB mice is discretely dysregulated and NR supplementation does not elicit robust proteomic changes

To profile the effects of NR in the hippocampi of this mouse cohort, we compared the proteome of 3xPB and HT animals, as well the NR-treated 3xPB with the untreated group. We again detected PZP to be upregulated in 3xPB hippocampi. NUDT3 was downregulated in 3xPB mice (Fig. 7A & 7B, Table S5). NUDT3 is a polyphosphate hydrolase which plays roles on DNA repair during oxidative stress response (Samper-Martín et al., 2021). Similarly to the cortex, the statistically significant protein differences after multi-testing correction remained null (Fig. 7C, Table S6). However, by filtering for the top 100 proteins

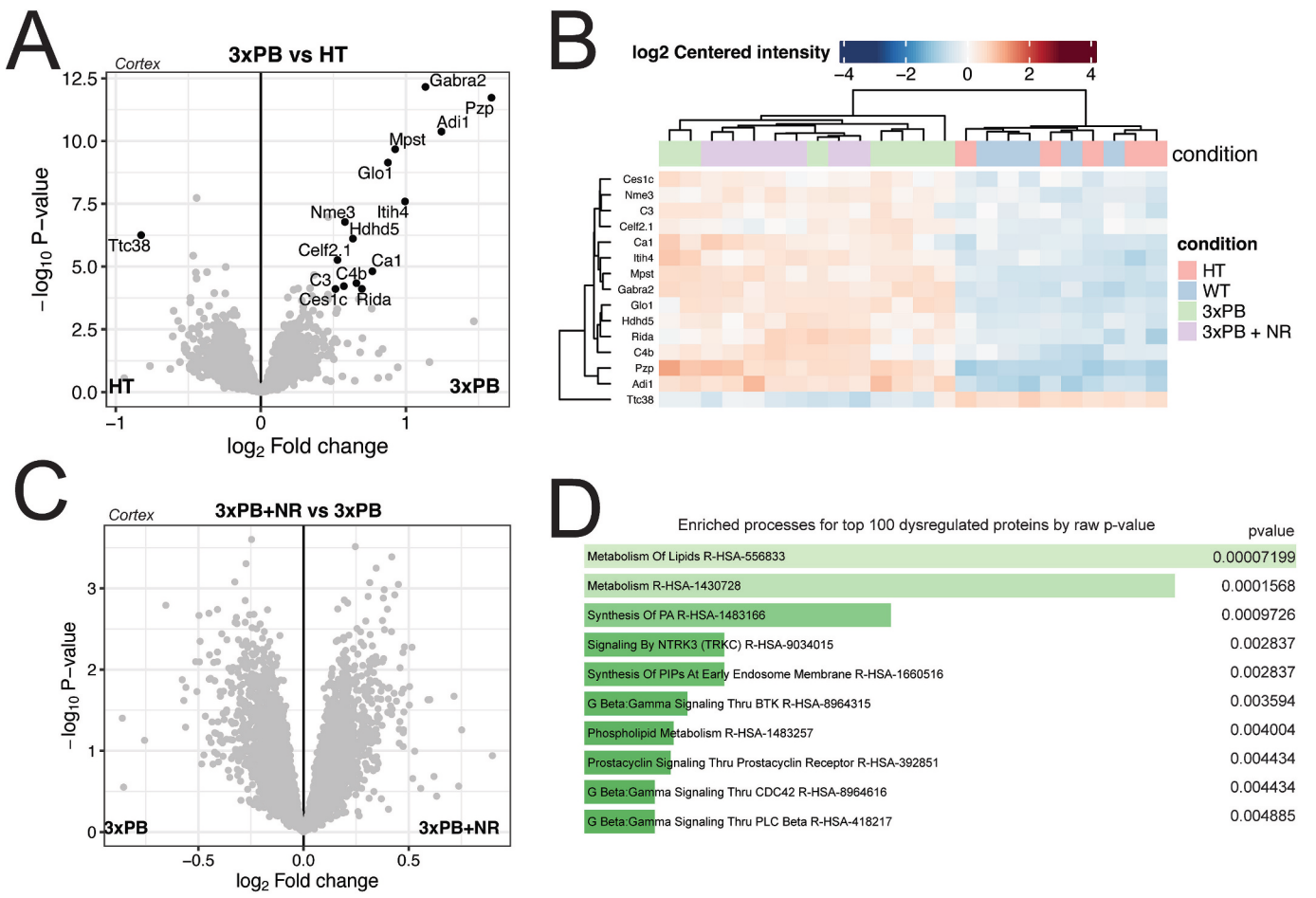

Fig. 6. Proteomic profiling of the 3xPB cortex and the effect of NR.
A. Volcano plot depicting differentially expressed proteins in the cortex of 3xPB and HT mice.
B. Heatmap depicting the proteomic abundances of CES1C, NME3, C3, CELF2, CA1,ITIH4MPST, GABRA2, GLO1, HDH5, RIDA, C4B, PZP ADI1 and TTC38.
C. Volcano plot depicting differentially expressed proteins in the cortex of NR-treated and untreated 3xPB mice.
D. Enriched processes from the top 100 significantly-different proteins by raw *p*-value.

with the smallest raw *p*-values (similarly to what we did for cortex), we observed enrichment of processes related to Citric Acid Cycle (TCA) and Respiratory Electron Transport and Complex I biogenesis, among others (Fig. 7D). Together these data point out at hippocampal proteomes being robust regardless of disease (for 3xPB) and that NR treatment may upregulate mitochondrial biogenesis in hippocampi of 3xPB mice.

2.10. Construction of weighted protein co-expression networks for cortex and hippocampi to investigate NR-induced proteomic modulations

The nature of the proteomic dataset makes it suitable to investigate co-expression networks (Johnson et al., 2022; Johnson et al., 2020; Langfelder and Horvath, 2008). Co-expression networks showcase the potential of describing gene or protein expression data to identify modules of co-expressed proteins across all samples and to correlate them to traits of interest relevant to our dataset. We then performed the weighted correlation network analysis (WGCNA) (Langfelder and Horvath, 2008) in the cortex and hippocampus datasets. We identified sets of modules that were co-expressed and correlated to the NR treatment and with certain traits of the RSI (Fig. 8A & 8C). We obtained modules that are arbitrarily labeled with colors before annotation (Table S7). We annotated these modules according to their top enrichment for GO Biological Processes. Within the cortex, the modules were labeled with different colors, such as black (cytoplasmic translation; GO:0002181), salmon (calcium ion transport; GO:1902514), turquoise (respiration; GO:0045333), greenyellow (neurotransmitter secretion; GO:0007269) and pink (Dephosphorylation: GO:0016311). These modules were negatively correlated with NR treatment in 3xPB mice. The modules brown (Peptide biosynthetic process; GO:0043043), magenta (aldehyde catabolic process; GO:0046185), midnightblue (Endomembrane System Organization; GO: 0010256) and grey60 (oxidative phosphorylation; GO:0006119 and phosphate metabolic process GO:0006796) positively correlated with NR treatment (Fig. 8B). Neurotransmitter secretion, aldehyde catabolic process, neurotransmitter secretion and respiration modules correlated with NR treatment and ATP abundance in the same manner, suggesting that these modules may contribute to ATP levels. Grey60 positively correlated with NR treatment and negatively correlated with ROS O_2^- and H_2O_2, highlighting the increase of oxidative phosphorylation with the decrease of ROS during NR treatment. Additionally, grey60 was negatively associated with H_2S, strengthening the opposite relationship between H_2S and oxidative stress (H_2S is an inhibitor of oxidative phosphorylation (Panagaki et al., 2019)).

For the hippocampus (Table S8), only the black module (Regulation of neurotransmitter receptor activity; GO: 0099601) was positively associated with NR treatment (Fig. 8C & 8D). NR has been shown to improve long-term potentiation in hippocampi (Yujun et al., 2018) and was associated with pathways related to neurotransmitters and synaptic function by microarray. Together, these data showcase the biological processes that may be involved in the changes of the RSI in the cortex of the NR-treated 3xPB mice.

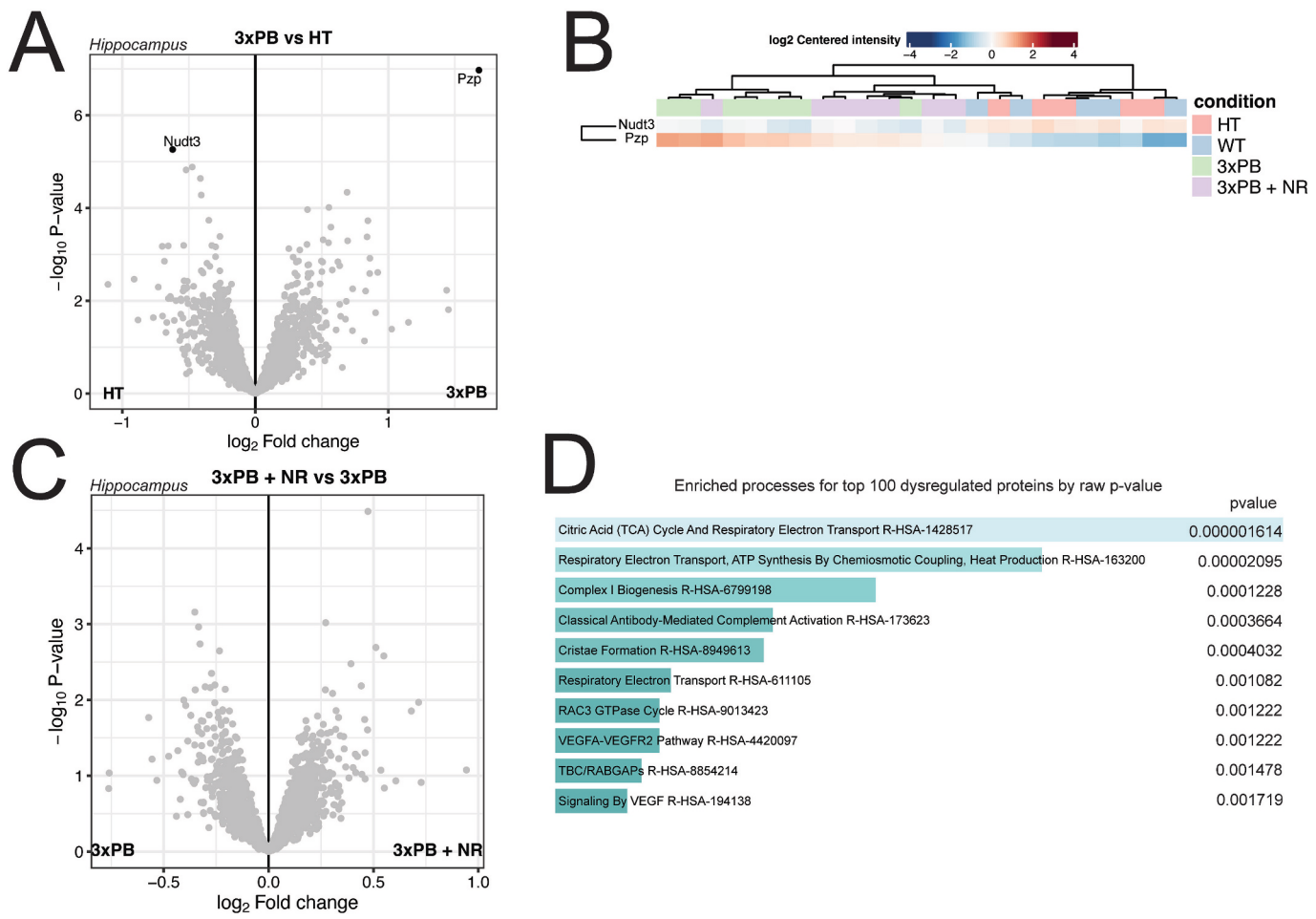

Fig. 7. Proteomic profiling of the 3xPB hippocampi.
A. Volcano plot depicting differentially expressed proteins in the hippocampi of 3xPB and HT mice.
B. Heatmap depicting the proteomic abundances of NUDT3 and PZP.
C. Volcano plot depicting differentially expressed proteins in the hippocampi of NR-treated and untreated 3xPB mice.
D. Enriched processes from the top 100 significantly-different proteins by raw p-value.

3. Discussion

In this study we have tested the protective potential of NR *in vitro* and *in vivo* in the context of oxidative distress. We performed a reactive species interactome profiling and correlated it to the proteomic landscape of an AD mouse model that recapitulates aging (3xPB). We have also profiled the effects of NR treatment on these mice. We observed discrete proteomic differences with robust reactive species modulation in a brain-area specific manner. These findings showcase that metabolic interventions may prove beneficial as disease-modifying therapies. The data generated here support the previously raised notion that the proteopathic nature of AD is not strictly disease-driving but concomitant. Our findings demonstrated that NR treatment can modulate several proteins related to aging and neurodegeneration, reactive species and brain-specific pathways related to AD pathology.

NR supplementation prevents ferroptosis in neurons *in vitro*. Beneficial effects of NR on AD fibroblasts were linked to the prevention of cytoplasmic DNA abundance (Hou et al., 2021) in these cells, preventing the activation of the cGAS-STING inflammatory signaling pathway. The cGAS-STING pathway is an innate immune system which detects double-stranded DNA (dsDNA) and leads to the transcription of type I interferons (IFNs) and IFN-stimulated genes (ISGs) by phosphorylation of STING (Cheng et al., 2020). Recent reports have linked ferroptosis and cGAS-STING pathways, with STING knockdown been shown to decrease ferroptosis sensitivity.

Reactive species determination exhibited brain-region-specific changes, with NR supplementation being able to attenuate oxidative distress in the cortex but not in the hippocampus. These results may reflect the different cellular compositions of both brain regions: comparable masses of cortex and hippocampus contain different amounts of soma and axons. There is experimental evidence that the cortex can withstand oxidative distress-inducing agents such as paraquat (Wang et al., 2009), while specific CA1 neurons in the hippocampus are more prone to oxidative stress-induced cell death (Wang et al., 2005). The specific RSI dysregulation in 3xPB mice and modulation with NR strongly suggest that notable redox enzymes such as SOD, catalase, myeloperoxidase, xanthine oxidoreductase or NOS activities may play a role in these RSI changes.

Some of the proteomic changes that we observed (GABRA2 and GLO1 upregulation) in the 3xPB mice have been identified on a spatial transcriptomic approach (Navarro et al., 2020). Whether the rest of dysregulated proteins have a transcriptomic dysregulation which drives increased or decreased protein expression remains to be investigated. Although the brain proteomes did not show multiple testing corrected differentially expressed proteins, the processes enriched by the top 100 proteins with smallest raw *p* value denoted important metabolic processes that may contribute to the RSI modulation. NR has been reported to modulate lipid droplet dynamics, which may be in line with these findings (Okur et al., 2023). For instance, upregulation of fatty acid metabolism could provide increased ATP, and it may contribute to the

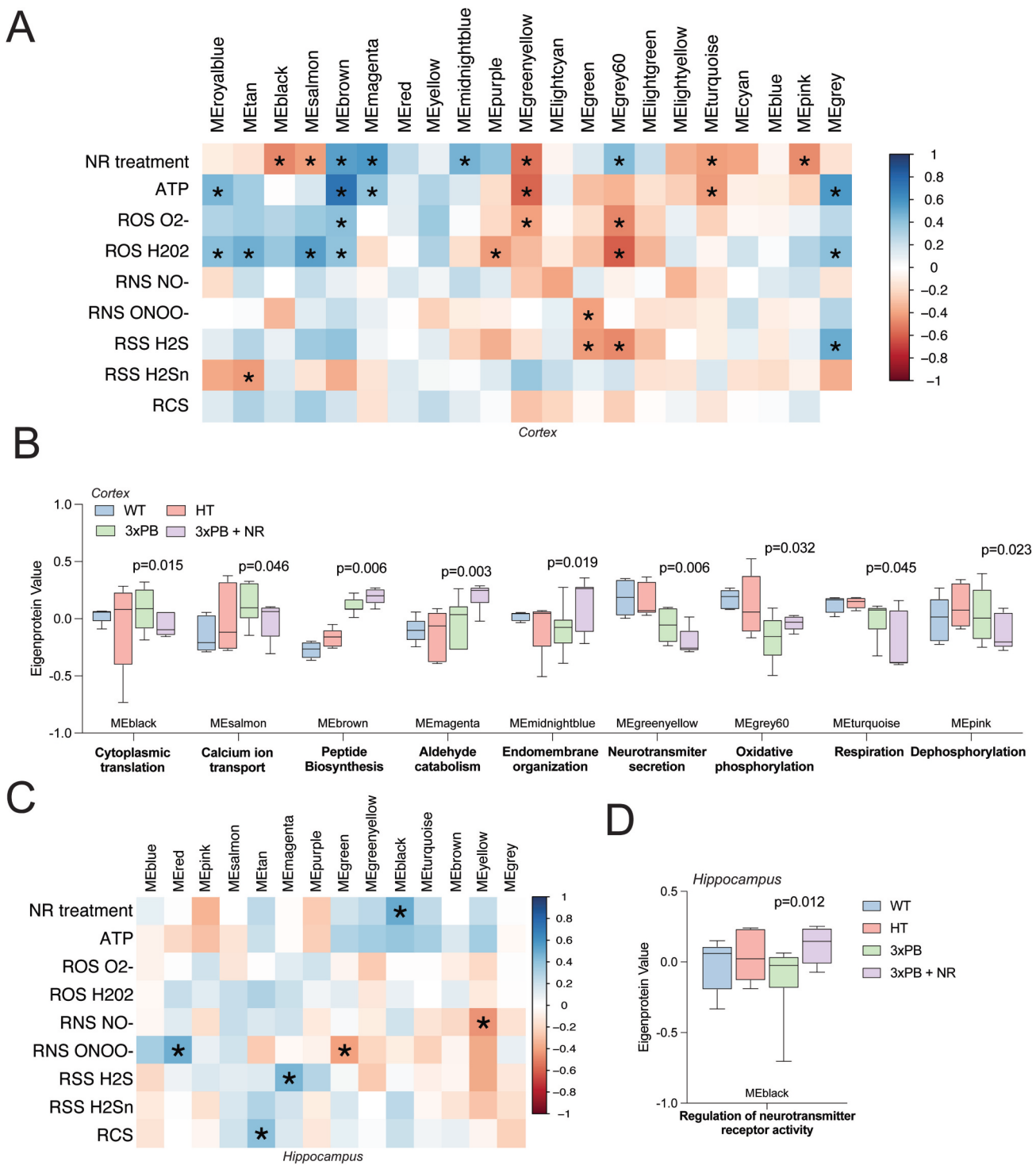

Fig. 8. Weighted co-expression protein networks for cortex and hippocampi.

A. Protein co-expression network for cortex built using WGCNA. Module relatedness is expressed in the heatmap depicting the correlation between the eigen value of the cluster (columns) and the trait of interest (in rows). In the case of the first row, the treatment with NR was a binary trait. All other traits were handled as continuous variables. Asterisk depicts a significant association of $p < 0.05$.

B. Module eigenprotein levels by condition for the nine NR-correlated modules.

C. Protein co-expression network for hippocampi built using WGCNA. Module relatedness is expressed in the heatmap epicting the correlation between the eigen value of the cluster (columns) and the trait of interest (in rows). In the case of the first row, the treatment with NR was a binary trait. All other traits were handled as continuous variables. Asterisk depicts a significant association of $p < 0.05$.

D. Module eigenprotein levels by condition for the only NR-correlated modules.

For B and D, data are presented as box plots and show the median and 25th and 75th percentiles, and box hinges represent the interquartile range of the two middle quartiles within a group. *P* values depicted in the plot are obtained from the WGCNA package for the association to NR treatment in 3xPB mice.

generation of ROS, and RCS production (Sandalio et al., 2023) in hippocampus, but not in the cortex. This may be due to a brain-region dependent vulnerability to reactive species stress.

Due to its beneficial effects on metabolism, NR and other NAD+ increasing therapies are being employed in clinical trials for AD (N-DOSE AD: NCT05617508; NCT04044131). With the present study, we propose that the reactive species interactome is modulated in disease and after NR treatment. Previously, Patel and colleagues reported *SOD1* downregulation in AD in a powerful transcriptomic meta-analysis of 22 datasets (Marmolejo-Garza et al., 2022; Patel et al., 2019). SOD expression and activity in AD cohorts may be related to brain-region specific changes and may segregate subjects in responders and non-responders. Measuring SOD expression and activity will contribute to the integral study of the AD patients.

The construction of protein co-expression networks for cortex and hippocampus of the aged mouse cohort contributes to the understanding of biological processes that occur upon NR treatment and which correlate to RSI dysregulations. To our knowledge, this is the first study that correlates proteomic modules of co-expression to the reactive species interactome. We employed the whole proteomic sample set but focused on the correlation to NR treatment. The reason for this is that modules of proteins that modulate their expression across oxidative distress-related aging (HT), AD background (3xPB) and NR treatment may be more meaningful and biologically relevant than only comparing the NR-treated and untreated mice.

It has been demonstrated that NR treatment has no effects on β amyloid deposition in 3xPB mice while preventing the behavioral and cognitive phenotype (Yujun et al., 2018). Our study continues to challenge the traditional amyloid-β-centric view of AD by demonstrating proteomic dysregulations and reactive species during disease onset and progression. An outlook for this field will be the investigation into the expression of the detoxifying enzymes of the RSI, the mitochondrial proteome and co-expression networks, which are warranted to uncover novel therapeutic targets or biomarkers and build personalized treatment strategies for AD.

4. STAR methods

4.1. Resource availability

4.1.1. Lead contact

Further information and request for resources and reagents should be directed to the lead contact, Amalia M. Dolga (a.m.dolga@rug.nl).

4.2. Materials availability

This study did not generate new unique reagents.

5. Experimental model details

5.1. Animals

All animal experiments were performed with the approval by the National Institute on Aging Animal Care and Use Committee. Mice were maintained on a standard NIH diet with a 12 h light/dark cycle at the National Institute on Aging and mice had access to food and water *ad libitum*. The CON mice were WT mice from the PolBHT strain (Sykora et al., 2015) plus four C57BL/6j mice from Jax. The 3xTgAD/HT PolB mice were as described by Sykora and colleagues (Sykora et al., 2015). All mice were on a C57BL/6 J background. Only female mice were used in these experiments, and they were group housed. CON WT mice were between 64 and 77 weeks old and HT PolB were between 64 and 74 weeks old. Control and NR-treated 3xTgAD/HT PolB were between 64 and 70 weeks old. NR-treated mice were given 12 mM NR (ChromaDex Inc) in their drinking water for 8 weeks prior to cull (Yujun et al., 2018) (Hou, 2018). NR water bottles were changed twice a week.

6. Method details

6.1. Tissue lysis

Mice were perfused with saline before sacrifice. Brain cortex and hippocampi were snap frozen in liquid nitrogen and stored at −80 °C until use. Protein extraction from brain cortex and hippocampus was performed with the lysis buffer 50 mM Tris·HCl pH 7.5, 150 mM NaCl, 1% Triton X-100, 0.1% SDS, on ice for 30 min. Extracted proteins were centrifuged to remove sample debris. The protein content was determined with the Bicinchoninic acid (BCA) Protein Assay (23,227, ThermoFisher Scientific/Pierce) and 20 μg of protein were loaded for SDS/PAGE.

6.2. Total ATP measurements

Total ATP content was measured with the CellTiter-Glo 2.0 Luminescent assay (G9241, Promega). All analyses were performed using freshly extracted total protein from brain cortex samples, and using microplate multimode reader Spark (Tecan).

6.3. Detection of the ROS $O_2^{\bullet-}$ and H_2O_2, RNS NO and $ONOO^-$, and the RSS H_2S and H_2S_n

Fluorescent molecules were used to measure ROS, specifically O_2^- (DHE, D7008, Sigma-Aldrich) and H_2O_2 (DCF-DA, D6883, Sigma-Aldrich), the RNS NO (DAF-2DA, AB145283, ABCAM) and $ONOO^-$ (DHR123, D1054, Sigma-Aldrich), the RSS H_2S (7-Azido-4-Methylcoumarin, 802,409, Sigma-Aldrich) and H_2S_n (Sulfane Sulfur Probe 4/SSP4, SB10–10, Tebubio), the RCS (4-Hydrazino-7-nitro-benzofurazan hydrazine adduct, 131,467–87-3, SantaCruz Biotechnology) in freshly extracted total proteins from brain samples. This was done by spectrofluorometry using a microplate multimode reader Spark (Tecan).

6.4. Proteomic analysis: sample preparation and analysis

Five μg (proteome) of each protein extract were prepared using a modified Gel-aided Sample Preparation protocol (Fischer and Kessler, 2015). Samples were digested with trypsin/Lys-C overnight at 37 °C. For nano-LC fragmentation, protein or peptide samples were first desalted and concentrated onto a μC18 Omix (Agilent) before analysis. The chromatography step was performed on a NanoElute (Bruker Daltonics) ultra-high-pressure nano flow chromatography system. Approximatively 200 ng of each peptide sample were concentrated onto a C18 pepmap 100 (5 mm × 300 μm i.d.) precolumn (Thermo Scientific) and separated at 50 °C onto a reversed phase Reprosil column (25 cm × 75 μm i.d.) packed with 1.6 μm C18 coated porous silica beads (Ionopticks). Mobile phases consisted of 0.1% formic acid, 99.9% water (*v*/v) (A) and 0.1% formic acid in 99.9% ACN (v/v) (B). The nanoflow rate was set at 250 nl/min, and the gradient profile was as follows: from 2 to 30% B within 70 min, followed by an increase to 37% B within 5 min and further to 85% within 5 min and reequilibration. MS experiments were carried out on a TIMS-TOF pro mass spectrometer (Bruker Daltonics) with a modified nano electrospray ion source (CaptiveSpray, Bruker Daltonics). A 1400 spray voltage with a capillary temperature of 180 °C was typically employed for ionizing. MS spectra were acquired in the positive mode in the mass range from 100 to 1700 *m/z* and 0.60 to 1.60 1/k0 window. In the experiments described here, the mass spectrometer was operated in PASEF DIA mode with exclusion of single charged peptides. The DIA acquisition scheme consisted of 16 variable windows ranging from 400 to 1200 m/z.

6.5. Proteomic analysis: protein identification

Database searching and LFQ quantification (using XIC) was performed using DIA-NN (version 1.6.0). An updated UniProt *Mus musculus*

database was used for library-free search / library generation. For RT prediction and extraction mass accuracy, we used the default parameter 0.0, which means DIA-NN performed automatic mass and RT correction. Top six fragments (ranked by their library intensities) were used for peptide identification and quantification. The FDR was set to 1% at the peptide precursor level. The variable modifications allowed were as follows: Nterm-acetylation and Carbamylation (RK). In addition, C-Propionoamide was set as fix modification. "Trypsin/P" was selected. Data were filtering according to a FDR of 1%. Cross-run normalisation was performed using RT-dependent.

6.6. Proteomic analysis: identification of differentially expressed proteins

To quantify the relative levels of protein abundance between different groups, datas from DIA-NN were then analysed using DEP package from R. Briefly, proteins that are identified in all samples were filtered, data were normalized using a variance stabilizing transformation and differential enrichment analysis was based on linear models and empherical Bayes statistic. DEP package provides fold increases, raw *p* values and FDR values (adjusted p values). After multitesting correction. we defined differentially expressed proteins as proteins with an absolute fold increase higher than 0.5 in relative abundance and p adjusted value smaller than 0.05. Results after differential expression are reported in the supplementary tables 1–6).

6.7. Building of a protein coexpression network with weighted gene correlation network analysis (WCGNA)

In order to generate a weighed protein co-expression network, we employed the WGCNA package in R. Briefly we employed the protein abundance matrixes per brain area sample set. Soft threshold power was determined for the dataset as a dataset-specific scale-free topology power based on: i) the power in a plot of power (x) *versus* R^2 (y) should be where the R^2 has approached an asymptote, usually near or above 0.80, and (ii) the mean and median connectivity at that power should not be exceedingly high, preferably around 100 or less. The WGCNA:: blockwiseModules() function was used with the following settings for the consensus network: Soft threshold power = 18, merge cut height of 0.25, type of mean topological overlap matrix as signed. Module composition is reported in Supplementary Tables 7–8. Eigenproteins per module were defined, which exhibit the most representative abundance value for a module which explains covariance of all proteins within each module. Gene ontology enrichment scores were calculated by inputing the lists of genes belonging to each module to EnrichR. Most significantly-enriched processes were employed for annotation of the protein model. Identified modules of proteins were correlated to NR treatment in the 3xPB groups, as well as the RSI abundances. Significant positive or negative correlations were summarized in the heatmap presented per brain area.

6.8. Primary cortical neuron culture

Primary cortical neurons (PCN) were prepared from C57BL/6 embryonic (E13–14) mice (mixed gender) under sterile conditions [39]. The cortex from embryos were collected and treated with 0.2 mg/ml trypsin at 37 °C for 15 min. After DNase and trypsin inhibitor treatment, the cell pellet was obtained through centrifugation. Neurobasal medium (#2508186; Gibco, Thermo Fisher Scientific, Netherlands) supplemented with 100 U/ml penicillin, 100 μg/ml streptomycin (#15070–063; Gibco, Thermo Fisher Scientific, Netherlands), 2 mM L-glutamine (#15070063; Gibco, Thermo Fisher Scientific, Netherlands) and 2% B27 supplement (#17504/044; Gibco, Thermo Fisher Scientific, Netherlands) was used to resuspend the cell pellet, followed by being seeded on PEI-coated (polyethylenimine, #P3143) 12-well Ibidi plates (30,000 cells/well). Experiments were performed on day *in vitro* (DIV) 7. Each experiment was independently repeated 3 times.

6.9. Calcein measurements on primary cortical neurons (PCNs)

On *in vitro* day 7, PCNs were treated for 24 h with RSL3 and NR (SMB00907, Sigma-aldrich). Neuronal network integrity was assessed with calcein-AM 1 uM and Hoechst 1 μg/uL (1 h incubation at 37 degrees in CO2 incubator). After 1-h, confocal microscopy images were acquired using Cell Discoverer 7 (Zeiss). A *Z*-stack was acquired, and a Maximum Intensity Projection was generated. Live cells are distinguished by the ubiquitous intracellular esterase activity, determined by the conversion of the cell-permeant calcein AM to the intensely fluorescent calcein. Every experiment comprised of 10 fields of view per condition and was repeated 3 times with similar results. A pooling of all measurements across experiments is shown.

7. Quantification and statistical analysis

Fig. 1 data are presented as violin plots depicting median, quartiles and data distribution. In Fig. 1 experiments, n defines the number of fields of view acquired. The statistical parameters can be found within the figure legends. To define differences between these four groups, two-way Analysis of Variance (ANOVA) was used with a Dunnett's multiple comparisons test. The criterion for significance was set at $p < 0.05$. Figs. 2–4 present data as mean ± SEM. Statistical parameters can be found within the figure legends. We employed ordinary one-way ANOVA with a Tukey's multiple comparisons test. The criterion for significance was set at $p < 0.05$. Statistical analyses were performed using GraphPad Prism 9 (San Diego, California). Box plots of Fig. 8 represent median values and 25th and 75th percentiles, and box hinges represent the interquartile range of the two middle quartiles within a group.

Key resources table.

REAGENT or RESOURCE	SOURCE	IDENTIFIER
Chemicals, peptides, and recombinant proteins		
Nicotinamide Riboside	ChromaDex Inc	
Nicotinamide Riboside Chloride	Sigma-aldrich	SMB00907
RSL3	Selleckchem	s8155
Critical commercial assays		
CellTiter-Glo 2.0 Luminescent assay	G9241	Promega
DHE	D7008	Sigma-Aldrich
DCF-DA	D6883	Sigma-Aldrich
DAF-2DA	AB145283	ABCAM
DHR123	D1054	Sigma-Aldrich
7-Azido-4-Methylcoumarin	802,409	Sigma-Aldrich
Sulfane Sulfur Probe 4/ SSP4	SB10–10	Tebubio
4-Hydrazino-7-nitro-benzofurazan hydrazine adduct	131,467–87-3	SantaCruz Biotechnology
Deposited data		
Proteomic raw data	This study	IPX0008924001
Code for proteomic analysis in R	This study	https://github.com/alejandromarmolejogarza/NR-effect-in-brain-proteome-and-RSI.git
Experimental models: Organisms/strains		
Control mice	The Jackson Laboratory	
HT PolB mice	Sykora et al., 2015	
3xTgAD/HT PolB mice	Sykora et al., 2015	
Software and algorithms		
Image J	NIH	https://imagej.nih.gov/ij/

(*continued on next page*)

(*continued*)

REAGENT or RESOURCE	SOURCE	IDENTIFIER
Graphpad Prism 9	www.graphpad.com	Graphpad Prism 9
R Software	R Core Team, 2013	https://www.r-project.org/
R Studio Software	RStudio Team, 2020	https://rstudio.com/
DEP package	Zhang et al., 2018	https://bioconductor.org/packages/release/bioc/html/DEP.html
WGCNA package	Langfelder & Horvath, 2008	https://rdrr.io/cran/WGCNA/

CRediT authorship contribution statement

Alejandro Marmolejo-Garza: Writing – original draft, Visualization, Methodology, Investigation, Formal analysis, Conceptualization. **Laurent Chatre:** Visualization, Resources, Methodology, Investigation. **Deborah L. Croteau:** Visualization, Methodology, Investigation. **Alejandro Herron-Bedoya:** Investigation. **Minh Danh Anh Luu:** Investigation. **Benoit Bernay:** Methodology, Investigation. **Julien Pontin:** Methodology, Investigation. **Vilhelm A. Bohr:** Writing – review & editing, Writing – original draft, Visualization, Resources, Methodology, Investigation, Conceptualization. **Erik Boddeke:** Writing – review & editing, Writing – original draft, Visualization, Resources, Methodology, Investigation, Conceptualization. **Amalia M. Dolga:** Writing – review & editing, Writing – original draft, Visualization, Resources, Methodology, Investigation, Conceptualization.

Declaration of competing interest

V.A.B. has CRADA arrangements with ChromaDex. All other authors declare no competing interests.

Data availability

Proteomic data have been deposited at iProX https://www.iprox.cn/ with the official number IPX0008924001 and are publicly available as of the date of publication. The code that supports the findings of this study can be found at github. https://github.com/alejandromarmolejogarza/NR-effect-in-brain-proteome-and-RSI.git (it is a private repository to be released once the study is published). Any additional information required to reanalyze the data reported in this paper is available from the lead contact upon request.

Acknowledgements

A.M.G is financially supported by the GSMS. A.M.D. is the recipient of an Alzheimer Nederland grant (WE.03-2018-04, The Netherlands), Parkinson Fonds (The Netherlands) and a Rosalind Franklin Fellowship co-funded by the European Union and the University of Groningen. This work was supported, in part, by the National Institutes of Health, National Institute on Aging. We thank Jane Tian and Sam Gray for their assistance with the mouse NR supplementation.

Appendix A. Supplementary data

Supplementary data to this article can be found online at https://doi.org/10.1016/j.nbd.2024.106645.

References

Beck, S. J., Mufson, J. E. & Counts, E. S. Evidence for mitochondrial UPR gene activation in familial and sporadic Alzheimer's disease. Curr. Alzheimer Res. 13 610–614 doi: https://doi.org/10.2174/1567205013666151221145445 (2016).

Bhatti, G.K., et al., 2022. Targeting mitochondrial bioenergetics as a promising therapeutic strategy in metabolic and neurodegenerative diseases. Biom. J. 45, 733–748.

Bjørklund, G., et al., 2022. the role of the thioredoxin system in brain diseases. Antioxidants 11. https://doi.org/10.3390/antiox11112161.

Cater, J.H., et al., 2019. Human pregnancy zone protein stabilizes misfolded proteins including preeclampsia- and Alzheimer's-associated amyloid beta peptide. Proc. Natl. Acad. Sci. 116, 6101–6110.

Chen, T., et al., 2023. Mitochondrial transplantation rescues neuronal cells from ferroptosis. Free Radic. Biol. Med. 208, 62–72.

Cheng, Z., et al., 2020. The interactions between cGAS-STING pathway and pathogens. Signal Transduct. Target. Ther. 5, 91.

Clémençon, B., Babot, M., Trézéguet, V., 2013. The mitochondrial ADP/ATP carrier (SLC25 family): pathological implications of its dysfunction. Mol. Asp. Med. 34, 485–493.

Curry, A.M., et al., 2023. Nicotinamide riboside activates SIRT5 deacetylation. FEBS J. 290, 4762–4776.

Daude, N., Gapeshina, H., Dong, B., Winship, I., Westaway, D., 2015. Neuroprotective properties of the PrP-like Shadoo glycoprotein assessed in the middle cerebral artery occlusion model of ischemia. Prion 9, 376–393.

Dolga, A.M., et al., 2013. Mitochondrial small conductance SK2 channels prevent glutamate-induced oxytosis and mitochondrial dysfunction. J. Biol. Chem. 288, 10792–10804.

Fang, E.F., et al., 2016. NAD+replenishment improves lifespan and Healthspan in Ataxia telangiectasia models via Mitophagy and DNA repair. Cell Metab. 24, 566–581.

Fischer, R., Kessler, B.M., 2015. Gel-aided sample preparation (GASP)—a simplified method for gel-assisted proteomic sample generation from protein extracts and intact cells. Proteomics 15, 1224–1229.

Fourcade, S., Ferrer, I., Pujol, A., 2015. Oxidative stress, mitochondrial and proteostasis malfunction in adrenoleukodystrophy: a paradigm for axonal degeneration. Free Radic. Biol. Med. 88, 18–29.

Gong, B., et al., 2013. Nicotinamide riboside restores cognition through an upregulation of proliferator-activated receptor-γ coactivator 1α regulated β-secretase 1 degradation and mitochondrial gene expression in Alzheimer's mouse models. Neurobiol. Aging 34, 1581–1588.

Honrath, B., et al., 2017. SK2 channels regulate mitochondrial respiration and mitochondrial Ca2+ uptake. Cell Death Differ. 1–13 https://doi.org/10.1038/cdd.2017.2.

Hou, Y., et al., 2021. NAD+ supplementation reduces neuroinflammation and cell senescence in a transgenic mouse model of Alzheimer's disease via cGAS–STING. Proc. Natl. Acad. Sci. 118, e2011226118.

Huang, L., et al., 2020. Intracellular amyloid toxicity induces oxytosis/ferroptosis regulated cell death. Cell Death Dis. 11, 828.

Johnson, E., et al., 2020. Large-scale proteomic analysis of Alzheimer's disease brain and cerebrospinal fluid reveals early changes in energy metabolism associated with microglia and astrocyte activation. Nat. Med. 26.

Johnson, E.C.B., et al., 2022. Large-scale deep multi-layer analysis of Alzheimer's disease brain reveals strong proteomic disease-related changes not observed at the RNA level. Nat. Neurosci. 25, 213–225.

Joy, J., et al., 2021. Proteostasis failure and mitochondrial dysfunction leads to aneuploidy-induced senescence. Dev. Cell 56, 2043–2058.e7.

Korovila, I., et al., 2017. Proteostasis, oxidative stress and aging. Redox Biol. 13, 550–567.

Kühl, I., et al., 2017. Transcriptomic and proteomic landscape of mitochondrial dysfunction reveals secondary coenzyme Q deficiency in mammals. Elife 6, e30952.

Langfelder, P., Horvath, S., 2008. WGCNA: an R package for weighted correlation network analysis. BMC Bioinformatics 9, 559.

Lin, X. *et al.* Contributions of DNA damage to Alzheimer's disease. Int. J. Mol. Sci. 21 Preprint at doi:https://doi.org/10.3390/ijms21051666 (2020).

Liu, D., et al., 2013. Nicotinamide forestalls pathology and cognitive decline in Alzheimer mice: evidence for improved neuronal bioenergetics and autophagy procession. Neurobiol. Aging 34, 1564–1580.

Maher, P., et al., 2018. The role of Ca2+ in cell death caused by oxidative glutamate toxicity and ferroptosis. Cell Calcium 70, 47–55.

Majerníková, N., den Dunnen, W.F.A., Dolga, A.M., 2021. The potential of ferroptosis-targeting therapies for Alzheimer's disease: from mechanism to transcriptomic analysis. Front. Aging Neurosci. 13 https://doi.org/10.3389/fnagi.2021.745046. Preprint at.

Malard, E., Valable, S., Bernaudin, M., Pérès, E., Chatre, L., 2021. The reactive species interactome in the brain. Antioxid. Redox Signal. 35, 1176–1206.

Marmolejo-Garza, A., et al., 2022. Transcriptomic and epigenomic landscapes of Alzheimer's disease evidence mitochondrial-related pathways. Biochim. Biophys. Acta 1869, 119326.

Marmolejo-Garza, A., et al., 2023. Negative modulation of mitochondrial calcium uniporter complex protects neurons against ferroptosis. Cell Death Dis. 14, 772.

Misrani, A., Tabassum, S., Yang, L., 2021. Mitochondrial dysfunction and oxidative stress in Alzheimer's disease. Front. Aging Neurosci. 13 https://doi.org/10.3389/fnagi.2021.617588. Preprint at.

Molenaars, M., Daniels, E.G., Meurs, A., Janssens, G.E., Houtkooper, R.H., 2020. Mitochondrial cross-compartmental signalling to maintain proteostasis and longevity. Philos. Trans. R. Soc. B 375, 20190414.

Navarro, J.F., et al., 2020. Spatial transcriptomics reveals genes associated with dysregulated mitochondrial functions and stress signaling in Alzheimer disease. iScience 23, 101556.

Nijholt, D.A.T., et al., 2015. Pregnancy zone protein is increased in the Alzheimer's disease brain and associates with senile plaques. J. Alzheimers Dis. 46, 227–238.

Okur, M.N., et al., 2023. Long-term NAD+ supplementation prevents the progression of age-related hearing loss in mice. Aging Cell 22, e13909.
Panagaki, T., Randi, E.B., Augsburger, F., Szabo, C., 2019. Overproduction of H2S, generated by CBS, inhibits mitochondrial complex IV and suppresses oxidative phosphorylation in down syndrome. Proc. Natl. Acad. Sci. 116, 18769–18771.
Patel, H., Dobson, R.J.B., Newhouse, S.J., 2019. A meta-analysis of Alzheimer's disease brain transcriptomic data. J. Alzheimers Dis. https://doi.org/10.3233/JAD-181085.
Pinho, B.R., et al., 2020. The interplay between redox signalling and proteostasis in neurodegeneration: in vivo effects of a mitochondria-targeted antioxidant in Huntington's disease mice. Free Radic. Biol. Med. 146, 372–382.
Richter, M., et al., 2015. SK channel activation modulates mitochondrial respiration and attenuates neuronal HT-22 cell damage induced by H2O2. Neurochem. Int. 81, 63–75.
Samper-Martín, B., et al., 2021. Polyphosphate degradation by Nudt3-Zn^{2+} mediates oxidative stress response. Cell Rep. 37.
Sandalio, L.M., Collado-Arenal, A.M., Romero-Puertas, M.C., 2023. Deciphering peroxisomal reactive species interactome and redox signalling networks. Free Radic. Biol. Med. 197, 58–70.
Swerdlow, R.H., Khan, S.M., 2004. A 'mitochondrial cascade hypothesis' for sporadic Alzheimer's disease. Med. Hypotheses 63, 8–20. https://doi.org/10.1016/j.mehy.2003.12.045.
Swerdlow, R.H., Burns, J.M., Khan, S.M., 2010. The Alzheimer's disease mitochondrial cascade hypothesis. J. Alzheimers Dis. 20, S265–S279.
Swerdlow, R.H., Burns, J.M., Khan, S.M., 2014. The Alzheimer's disease mitochondrial cascade hypothesis: progress and perspectives. Biochim. Biophys. Acta Mol. basis Dis. 1842, 1219–1231. https://doi.org/10.1016/j.bbadis.2013.09.010.
Sykora, P., et al., 2015. DNA polymerase β deficiency leads to neurodegeneration and exacerbates Alzheimer disease phenotypes. Nucleic Acids Res. 43, 943–959.
Trombetta-Lima, M., Sabogal-Guáqueta, A.M., Dolga, A.M., 2021. Mitochondrial dysfunction in neurodegenerative diseases: a focus on iPSC-derived neuronal models. Cell Calcium 94, 102362.
Vreones, M., et al., 2023. Oral nicotinamide riboside raises NAD+ and lowers biomarkers of neurodegenerative pathology in plasma extracellular vesicles enriched for neuronal origin. Aging Cell 22, e13754.
Wang, X., et al., 2005. High intrinsic oxidative stress may underlie selective vulnerability of the hippocampal CA1 region. Mol. Brain Res. 140, 120–126.
Wang, X., et al., 2009. Genomic and biochemical approaches in the discovery of mechanisms for selective neuronal vulnerability to oxidative stress. BMC Neurosci. 10, 12.
Weissman, L., et al., 2007. Defective DNA base excision repair in brain from individuals with Alzheimer's disease and amnestic mild cognitive impairment. Nucleic Acids Res. 35, 5545–5555.
Wilkins, H.M., Swerdlow, R.H., 2016. Relationships between mitochondria and neuroinflammation: implications for Alzheimer's disease. Curr. Top. Med. Chem. 16 (8), 849–857.
Xiong, F., Ge, W., Ma, C., 2019. Quantitative proteomics reveals distinct composition of amyloid plaques in Alzheimer's disease. Alzheimers Dement. 15, 429–440.
Yujun, H., et al., 2018. NAD+ supplementation normalizes key Alzheimer's features and DNA damage responses in a new AD mouse model with introduced DNA repair deficiency. Proc. Natl. Acad. Sci. 115, E1876–E1885.
Zhang, Q., et al., 2018. Integrated proteomics and network analysis identifies protein hubs and network alterations in Alzheimer's disease. Acta Neuropathol. Commun. 6, 19.